SF2A 2023
M. N'Diaye, A. Siebert, N. Lagarde, O. Venot, K. Baillié, M. Béthermin, E. Lagadec, J. Malzac, J. Richard (eds)

EXTENDED EMISSION IN SHORT GAMMA-RAY BURSTS FROM FALLBACK ACCRETION

R. Duqué[1], C. Musolino[1] and L. Rezzolla[1]

Abstract. Through a set of GRMHD simulations of BNS mergers, we reveal a long-lived phase of fallback accretion onto the merger remnant, totaling a mass of $\gtrsim 10^{-3} M_\odot$ over a time scale of hundreds of seconds. The accretion luminosity and timescale of the fallback points to the possibility that EM radiation from this inflow could explain long-term emission from BNS mergers, for example the extended emission of short GRBs. We devise a simple electromagnetic emission model based on the thermodynamical state of this material expected from its heating by r-process nucleosynthesis using the neutrino transport scheme of our GRMHD simulations. We find that this fallback material can shine in the gamma-rays and X-rays with luminosities $\gtrsim 10^{48}$ erg/s for hundreds of seconds. We predict that this emission is spectrally softer than prompt emission and that it ends in an exponential cutoff, features reminiscent of extended emission in GRBs. Finally, our findings suggest that the radiation from the fallback flow can impact the other electromagnetic signals from binary compact mergers, in particular the kilonova transient.

Keywords: GRMHD – Compact objects – Gravitational waves – Gamma-ray bursts

1 Introduction

The merging* of binary compact objects is a complex phenomenon involving many different physical processes, making them a great laboratory for many branches of physics and astrophysics (Baiotti & Rezzolla 2017). Nonetheless, the inspiral and merging processes are deterministic and determined by the parameters of the binary. In particular, the characteristics of the different outflows launched in the merger and their electromagnetic (EM) signals are fully determined by these binary parameters. The EM signals from binary neutron-star (BNS) mergers, as historically exemplified by the GW170817 event (The LIGO Scientific Collaboration et al. 2017; Abbott et al. 2017a), are an integral part of the rich phenomenology of short GRBs, that was explored before the GW era (e.g., Berger 2014; D'Avanzo 2015). All these signals likely arise from distinct outflows from the merger and the ideal tool to study the correspondence between outflows and EM signals is first-principle general-relativistic magnetohydrodynamical (GRMHD) simulations followed by adequate post-processing to implement the emission models of the EM counterparts.

In this contribution, we focus on the extended emission episodes of short GRBs (Norris & Bonnell 2006), that cover two recurring features in short GRBs observed in the gamma-ray and X-ray bands. Gamma-ray extended emission, first discovered in the prototypical GRBs 050724 and 060614 (Barthelmy et al. 2005; Gehrels et al. 2006), is a episode of gamma-ray emission that can last for hundreds of seconds after the prompt emission of short GRBs and that is of lower luminosity and softer spectrum than the parent prompt (a.k.a, "the spike"). It is present in 2–25% of short GRBs depending on the instrument.

The extended emission in the X-ray band was discovered in a sample of *Swift* sGRBs where the extended near-flat X-ray emission is suggested to be the X-ray counterpart of the extended emission in the gamma-rays (Kagawa et al. 2015). The X-ray extended emission has a similar duration (up to hundreds of seconds) and often features an exponential cutoff. X-ray extended emission is found in approximately 20–50% of short GRBs detected by *Swift* (Kisaka et al. 2017; Kagawa et al. 2019). In short GRBs with measured redshift, the

[1] Institut für Theoretische Physik, Goethe Universität Frankfurt am Main, D-60323 Frankfurt am Main, Germany

*The material of this contribution is drawn from a larger work on the extended emission of short gamma-ray busts in the light of a numerical study of fallback accretion in compact binary mergers, that is to be published shortly (Musolino, Duqué and Rezzolla, 2023).

© Société Française d'Astronomie et d'Astrophysique (SF2A) 2023

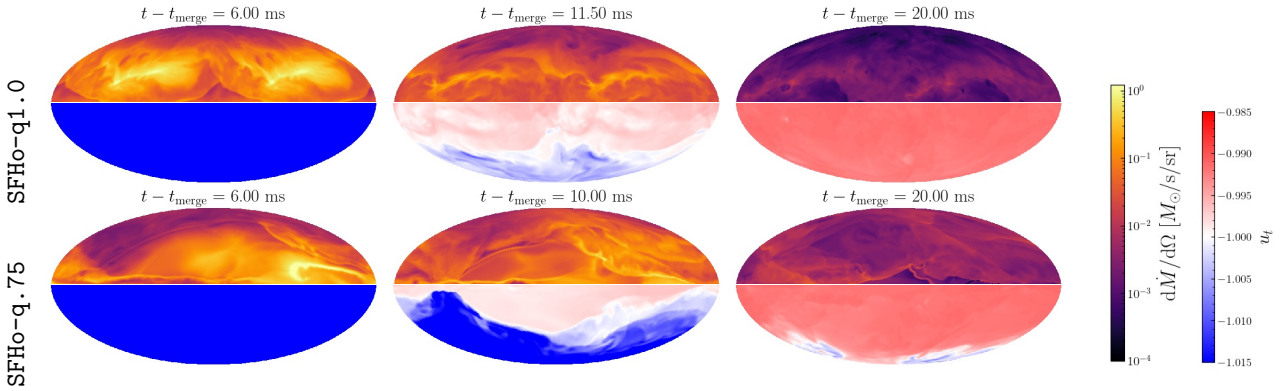

Fig. 1. Snapshots of the material flowing through a sphere at $R_d = 300\,M_\odot$ at various times of the simulation. **Upper panels:** `SFHo-q1.0` system. **Lower panels:** `SFHo-q.75` system. **Upper hemispheres:** mass flux per unit solid angle. **Lower hemispheres:** u_t of the flowing material. The three columns correspond to different times during the evolution, as reported in Fig. 2.

luminosities of extended emission episodes in the X-rays spans from 10^{46} to 10^{49} erg/s in the *Swift*/XRT band (Kisaka et al. 2017). The total output of extended emission episodes can largely exceed that of the prompt emission, suggesting a large reservoir of energy active on long timescales.

Extended emission in short GRBs has been understood through various pictures, invoking the launching of a second jet by the black hole (BH) central engine (Barkov & Pozanenko 2011), or radiation from a proto-magnetar central object (Bucciantini et al. 2012) or from material falling back after the burst (Kisaka & Ioka 2015). Indeed, the ejection of material that remains gravitationally bound to the central object and falls back on long time-scales seems to be ubiquitous in explosive events, from tidal disruption events (TDEs, Krolik & Piran 2012) to BNS mergers (Ishizaki et al. 2021).

In this contribution, we deepen the the study of extended emission from the fallback of merger ejecta using high-performance multi-physics numerical simulations including a novel scheme for neutrino transport.

2 A GRMHD study of long-term fallback episodes in BNS mergers

We perform state-of-the-art numerical relativity simulations of the binary inspiral and merger phases using the EinsteinToolkit framework (Löffler et al. 2012), the higher-than-second order accurate GRMHD module `FIL` (Most et al. 2019) and the recently developed moment-based neutrino transport module `FIL-M1` (Musolino & Rezzolla 2023). The inclusion of neutrino transport allows us to more accurately track the temperature and composition of the ejected and bound material, which are affected by weak interactions. We study four different systems with different mass ratio $q < 1$ and equation of state (EoS). For conciseness, we present here only two binary systems, both with the SFHo EoS (Hempel & Schaffner-Bielich 2010), a chirp mass equal to the estimated value for the GW170917 event (Abbott et al. 2017b), and two mass ratios $q = 1$ (system `SFHo-q1.0`) and $q = 0.75$ (`SFHo-q0.7`) consistent with the data from GW170817.

In Fig. 1, we present snapshots of the material outflowing from the merger at a distance of $R_d = 300\,M_\odot$ from the merger, at various times of our simulations of the two `SFHo` systems. The time-component of the material's four-velocity, u_t, determines whether the material is gravitationally bound or unbound, with a threshold at $u_t = -1$, as used in the color bar. Fig. 1 shows that the material initially ejected is unbound (left panel), and then progressively the ejecta is more and more bound. In addition, the front of bound material progresses from the equatorial region up to the polar directions, and ends up by filling the whole sphere. We also find that, while the early unbound ejecta is strongly anisotropic perhaps due to the tidal tails, the bound ejecta is quite isotropic. This can be seen at the maximum of bound mass ejection (middle panels), and even more at the later times (right panels). Comparing the upper and lower panels, we find that the asymmetry in the binary accentuates the anisotropy of the early unbound ejecta, as expected from its effect on the tidal tails, but has an opposite effect on the bound material, which is found to be even more isotropic than in the symmetric case. By analyzing the ejection latitudes θ of all the bound material detected in the simulation domain, we can confirm that the ejecta is isotropic, as suggested by the snapshots shown here.

In Fig. 2, we present the mass ejection history of our two systems, and we report the times at which the BH forms in the post-merger phase. This figure allows to confirm the trends found in the snapshots. For the

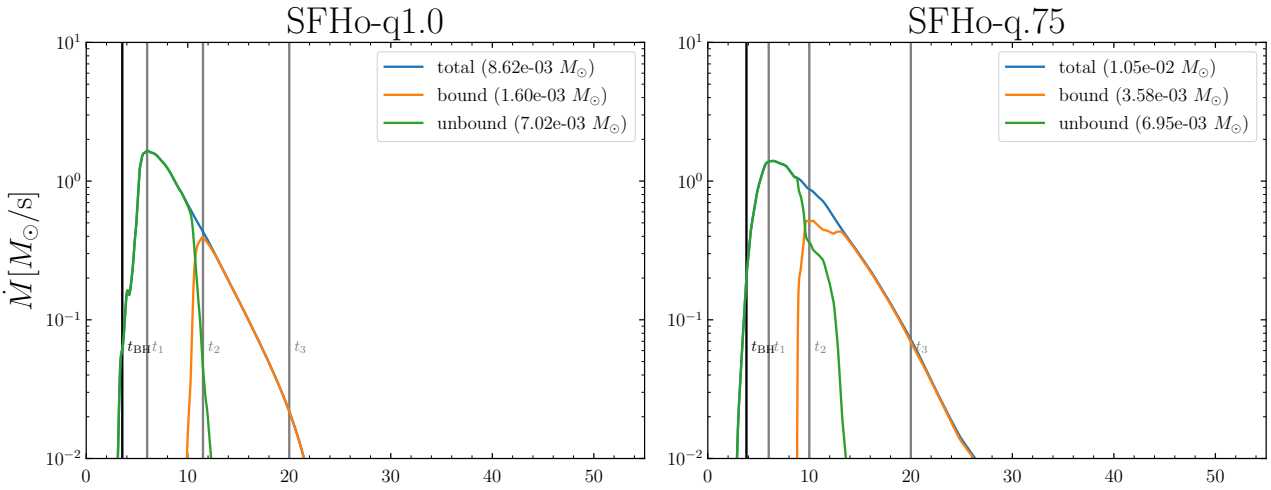

Fig. 2. Mass ejection history of two of our four simulations. All times are measured from the merger time, and the mass flux is separated into bound (orange), unbound (green) and total mass flux (blue). The legends report the total mass measured in all three categories. For all systems, the vertical gray lines mark the moments where the snapshots of Fig. 1 are taken. The time of BH formation is also marked, in black.

two `SFHo` systems, there is a sharp transition from unbound to bound ejection $\sim 10\,$ms post-merger. In the asymmetric binary, the decay of bound ejection is less steep than in the symmetric binary. Overall, the ejection episode is short-lived, due to the prompt collapsing of the BH $t_{\rm BH} \sim 4\,$ms post-merger and the very small disk mass $M_{\rm disk} \sim 2\,\% M_{\rm rem}$ susceptible of carrying our longer ejection. For the two prompt-collapse systems (`SFHo`), we find that asymmetry favors bound ejection, which is 19 % and 33 % of the total in the symmetric and asymmetric systems respectively.

This transition in time from unbound to bound suggests that the fallback material will remain *underneath* the unbound flow, with some physical separation. Inspecting the velocities of the bound and unbound component shows that, indeed, they should be well separated in the subsequent evolution, with consequences on the eventual radiation we explore in Sec. 4.

The dynamics of the bound matter on long-time scales cannot be followed exactly in our simulations for obvious computational reasons. Therefore, we consider Newtonian free-fall dynamics in the gravity filed of the remnant object, with the orbital period being $t_{\rm FB} = \frac{\pi}{\sqrt{2}} M |1+u_t|^{-3/2}$ for material with velocity u_t. Using the period of Newtonian orbits is justified by the length of the fallback orbits, since we are interested in timescales of hundreds of seconds. We determine the mass $M_{\rm rem}$ of the merger remnant using a quasi-local integral on the apparent horizon surface as determined by the vanishing of a null geodesic congruence expansion, or simply by measuring the gravitational field at a given distance using the metric components. We that these two methods agree to within 2%.

We find that the bond material in our simulations has fallback times up to hundreds of seconds. Together with the total mass of bound ejecta ($\gtrsim 10^{-3}\,M_\odot$, Fig. 2), this shows that the bound material can potentially contribute to a fallback episode on the remnant object and a long-term EM emission. To predict the fallback accretion rate, we study the the distribution of orbital energy ($\epsilon = -1 - u_t < 0$) per unit mass in the debris, denoted by $\mathrm{d}\epsilon/\mathrm{d}m_{\rm FB}$. Remarkably, this function is flat for a large range of energies, particularly, near the $\epsilon = 0$ bound, as hypothesized as early as Rees (1988); Evans & Kochanek (1989); Phinney (1989) in the study of fallback of debris from TDEs. Under this hypothesis, one has $\frac{\mathrm{d}m_{\rm FB}}{\mathrm{d}t_{\rm FB}} = \frac{\mathrm{d}m_{\rm FB}}{\mathrm{d}\epsilon}\frac{\mathrm{d}\epsilon}{\mathrm{d}t_{\rm FB}} \propto \frac{\mathrm{d}m_{\rm FB}}{\mathrm{d}\epsilon} \times t_{\rm FB}^{-5/3}$, such that the fallback accretion rate follows a power-law with $\dot{m}_{\rm FB} \propto t^{-5/3}$. This hypothesis was then indirectly confirmed by some later observations of TDEs (e.g., Komossa 2015). Our results thus show that, in addition to the tidal ejecta, the bound material of other origin such as from the merger itself and disk winds also verify this hypothesis.

Computing the fallback accretion rate confirms the power-law decay $\dot{m}_{\rm FB} \propto t^{-5/3}$, as had already been obtained in previous numerical studies of compact object mergers with various numerical schemes (Rosswog 2007; Chawla et al. 2010; Kyutoku et al. 2015). We here further confirm these results, and trace the origin

of the $t_{\rm FB}^{-5/3}$ behavior to the energy distribution of the ejecta. Using a crude conversion of accretion rate to luminosity, $L_{\rm acc} \sim 0.1 \times \dot{m}_{\rm FB} c^2$, we find that this inflow could sustain luminosities $L \gtrsim 10^{47}\,{\rm erg/s}$ for up to $\sim 1000\,{\rm s}$. This encourages us to better understand the radiation arising from this fallback accretion and its eventual observational signatures, as we do in Sec. 3.

3 From fallback accretion to extended emission in short GRBs

The fallback accretion rate determined in Sec. 2 is largely super-Eddington, such that a finer model for the fallback dynamics is required. In addition, one must account for the nucleosynthetic processes in the ejecta that contribute to the radiation from the fallback. To overcome the limitation in computational power, we derive a semi-analytical model to determine the fallback dynamics, from which a model for the radiation can be subsequently derived.

The material that falls back with $t_{\rm FB} \gtrsim 100\,{\rm s}$ has very eccentric orbits. Thus, we simplify our analysis by considering the inflow-outflow dynamics to be purely radial, in free-fall, with density and radial velocity fields $\rho(r,t)$ and $v(r,t)$ independent of the radial direction, following the isotropy of the ejecta underlined previously. The electron fraction of the material does depend on the latitude, and we will account for this in the determination of the fallback radiation below. In this free-fall flow, one can derive the following consistency equation connecting the density at any space-time point to that at a fiducial radius R_d:

$$\rho(R_1,t_1) = \left(\frac{R_d}{R_1}\right)^2 \rho(R_d, t_1 + t_{\rm FF}(R_1,R_d)) \times \left[1 + v_{\rm FF}(R_1,R_d)\frac{\partial t_{\rm FF}}{\partial R_i}(R_1,R_d)\right] \tag{3.1}$$

where $t_{\rm FF}(R_i,R_f)$ and $v_{\rm FF}(R_i,R_f)$ are the Newtonian free-fall time and free-fall velocity from radius R_i to R_f.

We solve for the density $\rho(r,t)$ with its non-trivial dynamics by enforcing the power-law fallback accretion rate $\dot{m}_{\rm FB} \propto t^{-5/3}$ at $R = R_d$, and using Eq. 3.1 to find the density throughout the ejecta. This, in turn, allows us to locate the photosphere, at radius $R_\phi(t)$, in the fallback flow. This is the position of the photosphere *within the fallback flow*, not accounting for the eventual unbound material above the flow.

At these early stages post-merger, the r-process nucleosynthesis is already well underway and the material opaque (e.g., Lippuner & Roberts 2015; Tanaka et al. 2020), though exact opacity calculations at these early times lack in the literature. Adopting a low opacity of $\kappa = 0.5\,{\rm cm^2/g}$, we find that for timescales up to $t \sim 10^5\,{\rm s}$, the photosphere coincides with the leading edge of ejecta, before starting to recede within the ejecta. We find the same with an opacity as low as $\kappa = 0.1\,{\rm cm^2/g}$. Therefore, we conclude that the radiation arising from the ejecta on these timescales comes from the leading-edge material, and we consider a black-body emission spectrum from this emitter. To capture the temperature time evolution $T_\phi(t)$ of this material accounting for r-process nucleosynthesis and expansion cooling, we run the `SkyNet` nuclear reaction network (Lippuner & Roberts 2017), with initial temperature and electron fraction determined from the neutrino scheme of our simulations, and with a density evolution at the photosphere according to our semi-analytical model $\rho(R_\phi(t),t)$.

In Fig. 3 (right panel), we report the bolometric, X-ray and gamma-ray luminosities of the fallback radiation according to our model. We considered the fallback material picked from latitude $\theta = 15\,{\rm deg}$ in the inflow. The initial Y_e of that material, also marked, is determined from our M1 scheme. The dotted line is the bolometric luminosity from the fallback accretion one would deduce from a naive conversion from the fallback rate $L_{\rm acc} = \eta \dot{m}_{\rm FB} c^2 \propto t^{-5/3}$, with an efficiency of $\eta = 10\%$.

First of all, we notice that the duration and luminosity of this radiation component are significant and on the level of extended emission in short GRBs (see Sec. 1). Second, we find that, through a non-trivial interplay between the photospheric radius and temperature evolution, the bolometric luminosity displays a power-law decay with near-constant slope $\alpha \sim -8/3$, which is steeper than the decay of $\dot{m}_{\rm FB} \propto t^{-5/3}$.

Because of the temperature's decreasing with time (we find $T_\phi \propto t^{-1}$, as in Wanajo et al. 2014; Lippuner & Roberts 2015), the radiation is mainly output first in the gamma-ray band, then in the X-ray band. In all bands, the luminosity follows three segments. At very early times, the blackbody temperature exceeds the energy band, such that the Rayleigh regime applies with $L_\gamma \sim R_\phi^2 T_\phi \propto t^{1/3}$. This near-constant segment of the light curve is apparent in the X-ray band in Fig. 3. Once the blackbody temperature reaches the observing band, at $t \sim 1\,{\rm s}$ for the gamma-rays, the luminosity follows the bolometric with $L_\gamma \propto t^{-8/3}$. Finally, the black-body peak frequency leaves the band, and an exponential cutoff is seen. In practice, the earlier segment of this sequence in the gamma-rays and the later segment in the X-ray are expected to be outshined by the prompt and the forward-shock afterglow respectively.

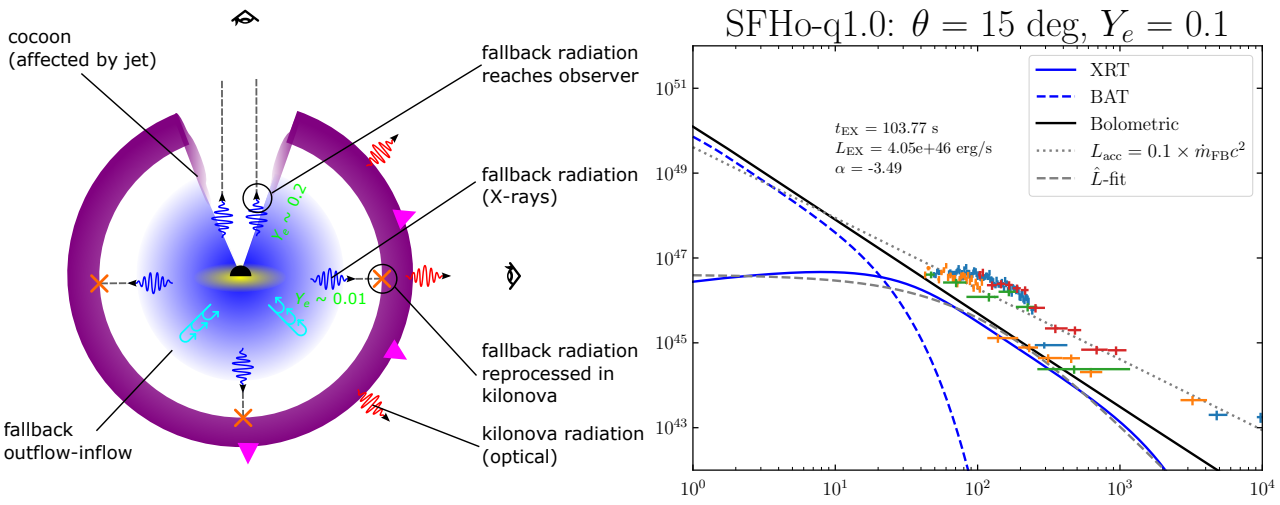

Fig. 3. Left: A schematic view of our model for the electromagnetic signature of the fallback flow. The fallback outflow-inflow (blue) is ejected underneath the unbound material (purple), where the kilonova signal is emitted (red photons). The fallback material emits X-rays (blue photons), that can either be absorbed and reprocessed in the kilonova ejecta (equatorial direction), or reach a distant observer by passing through the free way opened by the jet launched post-merger (polar direction). In this case, the fallback radiation appears as high-energy extended emission. **Right:** Radiation arising from the fallback flow as per our model of blackbody emission from the photosphere heated up by r-process nucleosynthesis (Sec. 3). The temperature evolution was determined from the r-process heating starting from the Y_e value measured at in the fallback flow, at the latitude indicated. We present the luminosity in the *Swift*/BAT and *Swift*/XRT bands (colored solid and dashed lines, respectively) and the bolometric luminosity (black solid line). We also present the luminosity derived from the accretion rate (gray dotted line) and the best-fit model of a flat-power-law light curve to the XRT luminosity (gray dashed line). Finally, we show the XRT data for some GRBs with extended emission in the source frame, arbitrarily scaled in flux to compare with our model (colored points, see text for the list of GRBs, data from Evans et al. 2007, 2009).

4 Discussion

4.1 A new high-energy emission component in BNS mergers

Our study suggests the general scenario for fallback radiation described in cartoon form in Fig. 3 (left panel).

On low-latitude or polar views of the binary merger, the fallback radiation to escape to a distant observer through the cavity opened by the jet or the lower optical thickness of the cocoon, i.e., a relatively low-density region where the jet has deposited energy in its interaction with the ejecta Bromberg et al. 2011; Matsumoto & Masada 2019. This makes up for a hitherto unconsidered emission component in BNS mergers, and a contender to explain the extended emission in short GRBs.

Indeed, the thermal spectrum and quickly decreasing hardness ratio of the radiation in our model reproduces an essential feature of extended emission in short GRBs: the relatively softer spectrum with respect to the parent prompt (Barthelmy et al. 2005; Gehrels et al. 2006; Kaneko et al. 2015). Moreover, the ratio of extended-emission energy to prompt energy in the gamma-rays varies in a large range, from $E_{EE}/E_{prompt} \lesssim 0.1$ to $\gtrsim 40$ (e.g. Bostancı et al. 2013; Kagawa et al. 2019). Beyond the uncertain geometrical factors that will condition the visibility of the fallback radiation in our scenario, our picture attributes these emissions to two distinct flows in BNS mergers, with energy output that are somewhat unrelated. Also, the initial Y_e of the bound material determines the temperature evolution and thus the time of the cutoff in the gamma-ray extended emission luminosity. The duration of the extended emission episode is thus, in our picture, weakly correlated with prompt emission temporal features, which remains to be explored in extended emission catalogs.

Turning to the X-ray component of extended emission, we note that the exponential cutoff, generally attributed to a black-hole spin-down in second-jet scenarios (Kagawa et al. 2015, 2019), is due in our picture to the crossing of the black-body peak frequency in the X-ray band. Again, this will occur sooner or later according to the heating rate in the bound material, such that we expect no strong correlation with the temporal properties

of the prompt emission.

To compare our model for extended emission with observations, we follow Kisaka et al. (2017) in fitting the *Swift*/XRT photometry expected from our model with a plateau of duration $t_{\rm EX}$ and luminosity $L_{\rm EX}$ followed by a power-law decay with a temporal index denoted by α. We find that the luminosity and durations of the plateau segment correspond to the clustering of the events reported in the Kisaka et al. (2017) catalog of events with redshift data. However, we find that the temporal slope is shallower than the $-40/9 \sim -4.4$ favored by Kisaka et al. (2017) corresponding to the second-jet model Kisaka & Ioka (2015). Indeed, we find the shallower $\alpha \sim -3.5$ in the case reported in Fig. 3 and in others, consistently with the temporal decay of the bolometric luminosity discussed previously.

To further ground our fallback emission model in the observations of extended emission, we place on the light-curve plots in Fig. 3 the data from extended emission in short GRBs 080905A, 080919, 150831A and 160821B. These were selected among the Kisaka et al. catalog to present a shallower decrease than the $-40/9$ that they use for their fits. This comparion shows that these shallow-decaying events are consistent with our model. Further, the data suggest that extended emission episodes show a variety of decay rates[†], implying that the universal $-40/9$ slope is not applicable, and that a diversity of physical mechanisms (such as fallback accretion and secondary BH jets) can be at the origin of the extended emission phenomenon. This non-uniqueness of the physical origin of extended-emission X-ray components is in line with the apparent bimodality in the duration and luminosity of these phenomena (Kisaka et al. 2017).

Finally, our picture for extended emission decouples the duration of the extended emission from the timescales of the small-scale physics near the remnant, in contrast with the magnetar and secondary-jet models (e.g., Barkov & Pozanenko 2011; Kisaka & Ioka 2015). Indeed, these models require the magnetar to shine (and to survive) of the jet to emit for as long as the emission lasts, up to hundreds of seconds. In our case, it is only the single and very short-lived process (the ejection of bound material over $t_{\rm ej} \lesssim 100\,{\rm ms}$) that results in a long-lived emission episode. The characteristics of this emission is largely set only from the very early post-merger dynamics. We have yet to study how this reconciles with the statistics of the duration of extended emission episodes.

4.2 Effect of the radiation from within the kilonova

Conversely, on high-latitude or equatorial directions, the fallback radiation is trapped by the kilonova material, and will not reach a distant observer. However, it will be absorbed and reprocessed, energizing the kilonova. Depending on the the radiative efficiency of the fallback flow and on the efficiency of reprocessing of this radiation into the kilonova emission, this effect can change the kilonova luminosity by roughly $\eta_{\rm FB} = m_{\rm FB}/m_{\rm KN}$, the ratio of fallback mass to unbound mass. This maximum ratio can reach $\sim 50\,\%$, though the effect on the kilonova luminosity is expected to be much less due to the low radiative and reprocessing efficiencies.

In the case of GW170817, Gill et al. (2019) used a series of GRMHD simulations to determine how long the remnant should have lasted to eject the large mass of lanthanide-poor (a.k.a, blue) component of the ejecta inferred from the kilonova signal ($M_{\rm blue} \sim 2 \times 10^{-2}\,M_\odot$; e.g., Perego et al. 2017; Villar et al. 2017). They concluded to a long-lived remnant collapsing after $t_{\rm collapse} \gtrsim 1\,{\rm s}$, a long timescale in apparent contradiction with the absence of very heavy elements in the kilonova composition (Perego et al. 2022), and possibly with the early launching of the jet in this system. Furthermore, simulations of BNS mergers suggest that only long-lived remnants are capable of ejecting this large mass of blue material (Fujibayashi et al. 2020). The proposal of a magnetar to energize the ejecta, softening the constraint on the blue mass (Metzger et al. 2018), likely also meets the challenge of the early launching of a jet by the magnetar. In this context, we note that energy injection from the fallback flow into the kilonova ejecta as described in our picture could contribute to alleviating the large-blue-mass constraint, and reconcile the data from GW170817 with a short-lived remnant able to launch a jet. We leave the investigation of this solution to future work.

5 Conclusion

Thanks to GRMHD simulations of the merger of binary neutron stars with neutrino transport, we have carried out a detailed study of the bound material ejected in the merger and post-merger phases. This component of the outflow is scarcely considered, and we reveal that it can have important a significant observational

[†]Some are very shallow (e.g., GRBs 060801, 061006, 100724A, 090426), others shallow (e.g, our selection of GRBs), others steep (e.g., GRBs 071227, 081023, 160821B).

signature in the gamma-ray and X-ray bands akin to extended emission episodes of short gamma-ray bursts, shining from within the expanding ejecta with luminosities $\sim 10^{50}$ erg/s over hundreds of seconds.

On lines-of-sight aligned with the binary's polar axis, looking through the funnel punched by the relativistic jet, this emission component is indeed a good candidate for the extended-emission of short gamma-ray bursts. On significantly misaligned lines-of-sight, this radiation is another source of energy injected into the ejecta and contributing to the kilonova counterpart. We see this process as a further complication in the inference of ejecta properties (e.g., mass and velocity) from kilonova data.

While the posr-processing of our simulations make simplifications in order to reach the actual light curve predictions for this emission component, the existence of this fallback flow is a robust result of our simulations, and the overall flux level of its radiation ($L \gtrsim 10^{46}$ erg/s) is largely determined by the mass of bound material, which is robustly determined from our simulations. Finally, the sharp cutoff of the radiation in the high-energy bands, due to the fast cooling of the ejecta, is an expected effect regardless of the details of the ejection.

RD, CM and LR are supported by the European Research Council Advanced Grant "JETSET: Launching, propagation and emission of relativistic jets from binary mergers and across mass scales" (grant no. 884631).

References

Abbott, B. P. et al. 2017a, Astrophys. J. Lett., 848, L13
Abbott, B. P. et al. 2017b, Phys. Rev. Lett., 119, 161101
Baiotti, L. & Rezzolla, L. 2017, Rept. Prog. Phys., 80, 096901
Barkov, M. V. & Pozanenko, A. S. 2011, MNRAS, 417, 2161
Barthelmy, S. D., Chincarini, G., Burrows, D. N., et al. 2005, Nature, 438, 994
Berger, E. 2014, Annual Review of Astron. and Astrophys., 52, 43
Bostancı, Z. F., Kaneko, Y., & Göğüş, E. 2013, MNRAS, 428, 1623
Bromberg, O., Nakar, E., Piran, T., & Sari, R. 2011, Astrophys. J., 740, 100
Bucciantini, N., Metzger, B. D., Thompson, T. A., & Quataert, E. 2012, MNRAS, 419, 1537
Chawla, S., Anderson, M., Besselman, M., et al. 2010, Phys. Rev. Lett., 105, 111101
D'Avanzo, P. 2015, Journal of High Energy Astrophysics, 7, 73
Evans, C. R. & Kochanek, C. S. 1989, Astrophys. J. Lett., 346, L13
Evans, P. A., Beardmore, A. P., Page, K. L., et al. 2009, MNRAS, 397, 1177
Evans, P. A., Beardmore, A. P., Page, K. L., et al. 2007, A&A, 469, 379
Fujibayashi, S., Shibata, M., Wanajo, S., et al. 2020, Phys. Rev. D, 101, 083029
Gehrels, N., Norris, J. P., Barthelmy, S. D., et al. 2006, Nature, 444, 1044
Gill, R., Nathanail, A., & Rezzolla, L. 2019, Astrophys. J., 876, 139
Hempel, M. & Schaffner-Bielich, J. 2010, Nuclear Physics A, 837, 210
Ishizaki, W., Ioka, K., & Kiuchi, K. 2021, Astrophys. J. Lett., 916, L13
Kagawa, Y., Yonetoku, D., Sawano, T., et al. 2019, Astrophys. J., 877, 147
Kagawa, Y., Yonetoku, D., Sawano, T., et al. 2015, Astrophys. J., 811, 4
Kaneko, Y., Bostancı, Z. F., Göğüş, E., & Lin, L. 2015, MNRAS, 452, 824
Kisaka, S. & Ioka, K. 2015, Astrophys. J. Lett., 804, L16
Kisaka, S., Ioka, K., & Sakamoto, T. 2017, Astrophys. J., 846, 142
Komossa, S. 2015, Journal of High Energy Astrophysics, 7, 148
Krolik, J. H. & Piran, T. 2012, Astrophys. J., 749, 92
Kyutoku, K., Ioka, K., Okawa, H., Shibata, M., & Taniguchi, K. 2015, Phys. Rev. D, 92, 044028
Lippuner, J. & Roberts, L. F. 2015, Astrophys. J., 815, 82
Lippuner, J. & Roberts, L. F. 2017, Astrophys. J., Supp., 233, 18
Löffler, F., Faber, J., Bentivegna, E., et al. 2012, Class. Quantum Grav., 29, 115001
Matsumoto, J. & Masada, Y. 2019, Mon. Not. R. Astron. Soc., 490, 4271
Metzger, B. D., Thompson, T. A., & Quataert, E. 2018, Astrophys. J., 856, 101
Most, E. R., Papenfort, L. J., & Rezzolla, L. 2019, Mon. Not. R. Astron. Soc., 490, 3588
Musolino, C. & Rezzolla, L. 2023, arXiv e-prints, arXiv:2304.09168
Norris, J. P. & Bonnell, J. T. 2006, Astrophys. J., 643, 266

Perego, A., Radice, D., & Bernuzzi, S. 2017, Astrophys. J. Lett., 850, L37

Perego, A., Vescovi, D., Fiore, A., et al. 2022, Astrophys. J., 925, 22

Phinney, E. S. 1989, in Proceedings of the 136th Symposium of the International Astronomical Union, held in Los Angeles, U.S.A., July 25-29, 1988, Vol. 136, The Center of the Galaxy, ed. M. Morris, 543

Rees, M. J. 1988, Nature, 333, 523

Rosswog, S. 2007, MNRAS, 376, L48

Tanaka, M., Kato, D., Gaigalas, G., & Kawaguchi, K. 2020, MNRAS, 496, 1369

The LIGO Scientific Collaboration, the Virgo Collaboration, Abbott, B. P., et al. 2017, Astrophys. J. Lett., 848, L12

Villar, V. A., Guillochon, J., Berger, E., et al. 2017, Astrophys. J. Letters, 851, L21

Wanajo, S., Sekiguchi, Y., Nishimura, N., et al. 2014, Astrophys. J., 789, L39